ACS OMEGA

http://pubs.acs.org/journal/acsodf

Article

Surface Passivation of Sputtered NiO_x Using a SAM Interface Layer to Enhance the Performance of Perovskite Solar Cells

Amira R. M. Alghamdi, Masatoshi Yanagida,* Yasuhiro Shirai,* Gunther G. Andersson, and Kenjiro Miyano

Cite This: *ACS Omega* 2022, 7, 12147−12157

Read Online

ACCESS | Metrics & More | Article Recommendations | Supporting Information

ABSTRACT: Sputtered NiO_x (sp-NiO_x) is a preferred hole transporting material for perovskite solar cells because of its hole mobility, ease of manufacturability, good stability, and suitable Fermi level for hole extraction. However, uncontrolled defects in sp-NiO_x can limit the efficiency of solar cells fabricated with this hole transporting layer. An interfacial layer has been proposed to modify the sp-NiO_x/perovskite interface, which can contribute to improving the crystallinity of the perovskite film. Herein, a 2-(3,6-dimethoxy-9*H*-carbazol-9-yl)ethyl]phosphonic acid (MeO-2PACz) self-assembled monolayer was used to modify an sp-NiO_x surface. We found that the MeO-2PACz interlayer improves the quality of the perovskite film due to an enlarged domain size, reduced charge recombination at the sp-NiO_x/perovskite interface, and passivation of the defects in sp-NiO_x surfaces. In addition, the band tail states are also reduced, as indicated by photothermal deflection spectroscopy, which thus indicates a reduction in defect levels. The overall outcome is an improvement in the device efficiency from 11.9% to 17.2% due to the modified sp-NiO_x/perovskite interface, with an active area of 1 cm^2 (certified efficiency of 16.25%). On the basis of these results, the interfacial engineering of the electronic properties of sp-NiO_x/MeO-2PACz/perovskite is discussed in relation to the improved device performance.

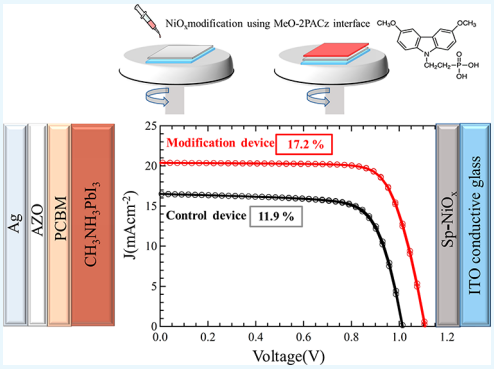

1. INTRODUCTION

Perovskite solar cells (PSCs) offer several advantages because of their ease of fabrication, low cost, and ability to produce transparent, flexible devices with good quality on a laminated output.[1,2] The device performance of PSCs with inverted structure is influenced by the hole transport layer (HTL). Some semiconductor materials that are used as hole transport materials (HTMs) in PSCs have attracted the attention of researchers; these materials include PEDOT:PSS, CuO, graphene oxide, V_2O_5, PbS, and PTAA (poly(bis(4-phenyl)-(2,4,6-trimethylphenyl)amine)).[3−7] The main reasons for preferring these inorganic HTMs over organic HTMs are the higher hole transporting ability, higher stability, and lower cost of manufacturing of the first.

Notably, NiO_x has been successfully applied as a wide bandgap (3.6−4.0 eV) p-type semiconductor material in an inverted structure.[8−10] The preference of NiO_x is based on its intrinsic properties, including suitable work function and adequate charge carrier mobility, which can sufficiently match the energy level of perovskites by adjustment of the O^{2-} or Ni^{2+} concentration.[11−14] Another advantage of NiO_x is that multiple methods are applicable and available for its deposition,[15−17] whereby sputtering offers suitable control of the composition of NiO_x, allowing for roll-to-roll fabrication.[18,19] Perovskite based on sputtered NiO_x (sp-NiO_x) can show an operational stability as high as 4000 h.[20] According to its stoichiometry,[21] NiO_x is a Mott−Hubbard insulator. However, nonstoichiometric composites (such as NiOOH and Ni_2O_3, and Ni^{3+} species) can be induced by the oxidation of NiO_x, which significantly improves the p-type conductivity.[19]

Pristine NiO_x has low conductivity, which may degrade hole extraction by aggravating charge carrier recombination.[22] Consequently, methods to increase the conductivity of NiO_x have emerged for treating NiO_x.[11,23−25] Notably, nickel vacancies dominate the p-type conduction in nontreated NiO_x.[26] Moreover, the internal p-type conductivity is limited because the Ni vacancies in untreated NiO_x have a large ionization energy. Consequently, extrinsic treatments such as dopants, which contain shallow acceptor levels, are preferred,[27] helping to increase the conductivity of NiO_x and, thus, yielding enhanced PSCs.[24,28−30]

Received: January 25, 2022
Accepted: March 11, 2022
Published: March 30, 2022

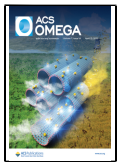

https://doi.org/10.1021/acsomega.2c00509
ACS Omega 2022, 7, 12147−12157

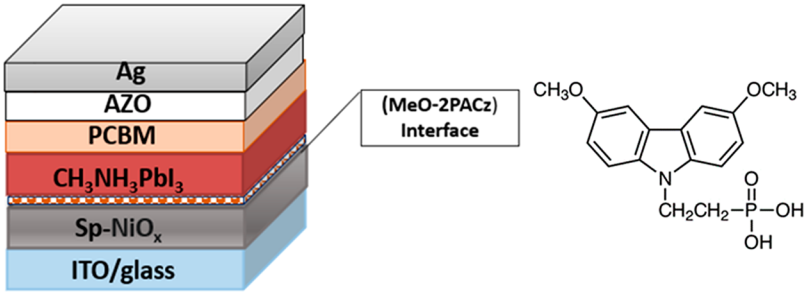

Figure 1. Schematic representation of the device structure and chemical structure of MeO-2PACz.

In addition, the charge carrier transfer is significantly affected by the interface defects/traps occurring between the NiO_x and perovskite layers because charge extraction takes place at the interface, which suffers from charge recombination.[31] These defects may be minimized by introducing a layer between perovskite and NiO_x. Moreover, the introduced interface layer improves energy level matching; hence, this has become a preferred method for realizing further improvement of PSC performance.[32] Furthermore, self-assembled monolayers (SAMs) form layers by the self-assembly of surfactant molecules at surfaces. SAMs are capable of being physisorbed or chemisorbed onto a number of surfaces and forming extremely thin layers when they are applied using solution-processed techniques, such as dip coating, slot-die coating, blade, spraying, and spin coating.[33] Surface modification using SAM has been widely applied in PSCs.[34−36] Consequently, SAM-based HTL for inverted perovskite solar cells have been used[37−39] and helped in achieving 21% efficiency for a single-junction device.[40]

Bai et al.[41] modified a NiO_x crystal film surface using a small molecule (diethanolamine). As a result, the chemical reaction rate of the conversion of PbI_2 to $MAPbI_3$ ($MA^+ = CH_3NH_3^+$) was slowed, creating a better interface and film quality. Zhang et al.[42] focused on reducing trap-assisted recombination between the NiO_x and perovskite layer by introducing ferrocenedicarboxylic acid (FDA) to modify NiO_x. Hence, the modifications yielded improved power conversion efficiencies (PCEs) to 18.2% with improvement of the crystallization of the perovskite layer, hole transport, and collection abilities. Furthermore, the resulting PSCs were stable, which concurs with another modification that was performed using ferrocenedicarboxylic acid and PTAA. This modification attained better perovskite films with efficient hole extraction.[43] To passivate the NiO_x surface, Wang et al.[32] investigated a series of para-substituted benzoic acid (R-BA) SAM layers on NP NiO_x. As result, the devices that included SAM had PCEs of 18.4% and were less affected by trap-assisted recombination, minimized energy offset between NiO_x NP and perovskite, and changed the surface wettability.

Recently, it has been shown that modification of NiO_x is the key challenge to improve the open-circuit voltage (V_{oc}) by reducing the defects of NiO_x.[44−46] In addition, to reduce the surface defect and hydroxyl group presented on NiO_x, Mann et al. used 3-(triethoxysilyl)propylamine (TSPA) as the SAM between NiOx and perovskite. They found that SAM passivated the surface of NiO_x and reduced the recombination of the charge.[47]

A new generation of SAM, [2-(3,6-dimethoxy-9*H*-carbazol-9-yl)ethyl]phosphonic acid (MeO-2PACz), was developed for the first time by Al-Ashouri et al. as a hole-selective contact with intrinsic scalability, ease of processing, low cost, and free of dopants. Another improvement entails enabling highly efficient p−i−n PSCs and a record-efficiency monolithic perovskite/CIGSe tandem device.[48] Furthermore, selecting SAMs for application in perovskite devices is an important factor, whereby ([2-(9*H*-carbazol-9-yl)ethyl]phosphonic acid) (2PACz) and ([2-(3,6-dimethoxy-9*H*-carbazol-9-yl)ethyl]-phosphonic acid) (MeO-2PACz) can create an interface that is energetically well aligned with the perovskite absorber with minimal nonradiative recombination.[48] After this work, they further designed a tandem perovskite solar cell using the same SAM (MeO-2PACz) and found that a fast hole extraction was linked to a low ideality factor.[49] They also investigated the ITO surface coverage using MeO-2PACz on the top surface and introduced NiO as the intermediate layer.[40] Lastly, Sun et al. developed a method to enhance the interaction between MeO-2PACz and ITO using a sputtered NiOx layer with triple-cation perovskite devices. The result shows that NiO_x passivates the ITO and prevents direct contact between perovskite and ITO, which contributes to improving the PCE.[50] Herein, we developed a similar strategy using sp-NiO_x by coating MeO-2PACz on top of sp-NiO_x to study the surface defect of NiO_x and perovskite interfaces using different analytical techniques with the commonly used perovskite methylammonium lead iodide (MAPbI3). Despite these remarkable contributions, the application of MeO-2PACz, by modulating the crystal contact or layer between NiO_x/perovskite, needs more investigation. Therefore, the current study involves a systematic investigation of the effect of MeO-2PACz on a NiO_x layer. Second, an in-depth analysis of the defect at NiO_x and perovskite layers is conducted, whereby a thin layer of MeO-2PACz is inserted, as illustrated in Figure 1.

The surface functional groups of NiO_x are composed of hydroxylated groups[51,52] that react with phosphonic groups.[41,53] Hence, the three main goals of using a SAM include the following: First, a SAM can synchronously contribute to improving the crystallinity and stability of the perovskite layer. Second, a SAM should be able to passivate the defects of the interface. Third, a SAM can be applied to have superior interface contact properties compared to the plain NiO_x layer. The current work shows that MeO-2PACz reduces the defects in sp-NiO_x and enhances the quality of the perovskite film by enlarging the domain size, increasing the charge attraction efficiency, and reducing charge recombination. In this case, PSCs with a modified sp-NiO_x/perovskite interface yielded PCEs of 17.2% with an active area of 1 cm^2 (certified efficiency of 16.25%, Figure S3). Therefore, the outcome proves that it is feasible to treat the sp-NiO_x/perovskite interface because the performance of PSCs with a sp-NiO_x HTL is significantly improved.

https://doi.org/10.1021/acsomega.2c00509
ACS Omega 2022, 7, 12147−12157

2. EXPERIMENTAL SECTION

2.1. Structure of the Device. The device containing the SAM interface had the following structure: ITO-coated glass/sp-NiO_x/MeO-2PACz/perovskite and $(CH_3NH_3PbI_3)$/$PC_{61}BM$/aluminum-doped zinc oxide (AZO)/Ag, which is illustrated in Figure 1. In this representation, sp-NiO_x acts as the HTL layer, which blocks electrons, and $PC_{61}BM$/AZO acts as the electron transport layer.

2.2. Hole Transport Layer Deposition. A radiofrequency sputtering method was applied to deposit the 20 nm NiO_x hole transporting layer onto indium tin oxide (ITO) glass (10 ± 2 ohm/square, Ra < 2.6 nm) at room temperature. The radio frequency (RF) sputtered equipment was obtained from Sanyu Electron Co., Ltd., Tokyo, Japan, SVC-700 RF II NA. Commercially available 99.9% pure NiO (Kojundo Chemical Lab. Co., Ltd., Saitama, Japan) was used as the target, and the sputtering was done at 3.5 Pa argon pressure. The sputtering chamber was evacuated to reach less than 2×10^{-3} Pa before the deposition.

2.3. Self-Assembly Monolayer Deposition. The glass substrate with sputtered NiO_x was brought inside a glovebox. SAM preparation utilized MeO-2PACz (TCI, >98.0%) (6 mg) dissolved in 18 mL of ethanol. Extra care was taken to prevent particle formation, whereby all solutions were prepared inside a glovebox and filtration was carried out using 0.22 μm syringe filters. The next step was to spin coat the MeO-2PACz over sp-NiO_x HTL at 3000 rpm for approximately 30 s. Annealing was performed for 10 min on a hot plate (100 °C). The perovskite film deposition entailed two steps, starting with spinning.

2.4. Perovskite Layer Deposition. Perovskite layer deposition began with the preparation of the perovskite precursor solutions, whereby 5-AVAI (5-aminovaleric acid hydroiodide) (6.3 mg) and PbI_2 (Kanto Chemical, 98% purity) (1260 mg) were dissolved in DMF−DMSO (2.85−0.15 mL). Methylammonium chloride (MACl) (Wako Chemicals, battery grade]) (5 mg) and methylammonium iodide (MAI) (Wako Chemicals) (95 mg) were dissolved in 2 mL of ethanol and then stirred overnight at 300 rpm/70 °C. Subsequently, spin coating was performed by preparing perovskite using a two-step interdiffusion method; more details can be found in our previous work.[54] The perovskite films were deposited in two steps, starting with spin coating PbI_2 solution onto MeO-2PACz (3000 rpm, 30 s), annealing for 3 min on a hot plate (100 °C) and spin coating the MAI solution (4000 rpm, 30 s) as a second step. The films obtained were then annealed under a methylammonium chloride (MACl) vapor environment to improve the perovskite film.[55]

2.5. Electron-Transport Layer and Metal Electrode Deposition. Preparation of the metal electrode and electron transport layer began by dissolving phenyl-C_{61}-butyric acid methyl ester ($PC_{61}BM$) in 20 mg/mL of chlorobenzene, which was followed by spin coating over the previously prepared perovskite films (1000 rpm, 7 s, then 3000 rpm for 30 s). Thereafter, the samples were annealed at 100 °C for 15 min. To spin coat aluminum-doped zinc oxide (AZO) (Avantama AG (N-21X)), the AZO solution was placed onto the $PC_{61}BM$ layer (1500 rpm, 5.5 s, then 4000 rpm, 20 s), which was followed by annealing on a hot plate (100 °C, 10 min). The cells were completed by thermally evaporating 150 nm thick Ag electrodes. The final step of the process involved encapsulation with cavity glasses, which were sealed using ultraviolet curable resins, including UVRESIN XNR5516Z, NagaseChemteX, Japan.

2.6. Characterization. X-ray diffraction (XRD) patterns were obtained using a Bruker D8 advanced X-ray diffractometer, Cu Kα radiation, λ = 1.54050 Å, with a scan rate set at 3° min^{-1}. A field emission scanning electron microscope (Hitachi S-4800) was used to capture a morphological image of the films, and the accelerating voltage was set to 5 kV. An ultraviolet−visible−near-infrared spectrometer (7200, V-JASCO) was used to measure the absorption and transmittance spectra. Moreover, a spectrofluorometer (FP8500, JASCO) was used to obtain the photoluminescence (PL) spectra. The time-resolved photoluminescence (TRPL) was measured with a fluorescence lifetime spectrometer (Quantaurus-τ from Hamamatsu-Photonics K.K.) equipped with ∼405 nm laser diode (typical peak power of 400 mW) at 200 kHz repetition rate. Another characterization step entailed carrying out X-ray photoelectron spectroscopy using a Versa Probe II (ULVAC-PHI, Japan). The current density−voltage (J−V) curves were measured under 1 sun using an AM 1.5G spectral filter with an active area of 1 cm^2, which was calibrated by a silicon reference cell. A spectrometer (SM-250IQE, Bunkokeiki, Japan) was used to characterize the incident monochromatic photon-to-electron conversion efficiency (IPCE) spectra, calibrated by a silicon reference cell. Photothermal deflection spectroscopy (PDS) was used for different treatments of the NiO_x surface to characterize the defect levels present in the perovskite/NiO_x and NiO_x/ITO bandgaps. PDS is a suitable method because it enables the detection of the defect levels for all charge states within the measured sample depth; it detects the charge states in accordance with the absorption coefficient.[56−58] In this case, monochromatic light was used to irradiate the sample surface. The light source was a halogen lamp modulated at a chopping frequency ranging between 7 and 11 Hz with incident light at a normal angle to the sample surface. A filter was fixed and used to facilitate the measurement over a wavelength range from 700 to 1200 nm. The previous pumping light was concentrated using a cylindrical lens. The dimensions of the lens were 1 × 10 mm^2. A semiconductor laser (660 nm) was then used to probe the sample surface in parallel with the light. During probing, the laser was deflected based on the thermal energy produced by the combination of the electrons activated by the pump light. During the process, there was a need to enhance the deflection of the laser probe. This was achieved by conventionally dipping the PDS sample into a fluorinert (FCI) solution characterized by a high coefficient-of-temperature dependence of the refractive index, $\delta n = \delta T$, where T and n represent the temperature and refractive index, respectively.

Finally, photoelectron spectroscopy was applied using an ultrahigh vacuum (UHV). X-ray photoelectron spectroscopy (XPS) with a nonmonochromatic source was measured (Al Kα; 1486.6 eV, spot size; 10—300 mm) at a pass energy of 10 eV. XPS was used to determine the composition and chemical state of the components for depths of up to 10 nm.

3. RESULTS AND DISCUSSION

3.1. Understanding the Effect of MeO-2PACz (SAM) on the NiOx Layer. A correlative investigation was conducted into the impact of the MeO-2PACz (SAM) interface on NiO_x and its influence on the performance of a solar cell device. Hence, the focus is to understand the properties and

https://doi.org/10.1021/acsomega.2c00509
ACS Omega 2022, 7, 12147−12157

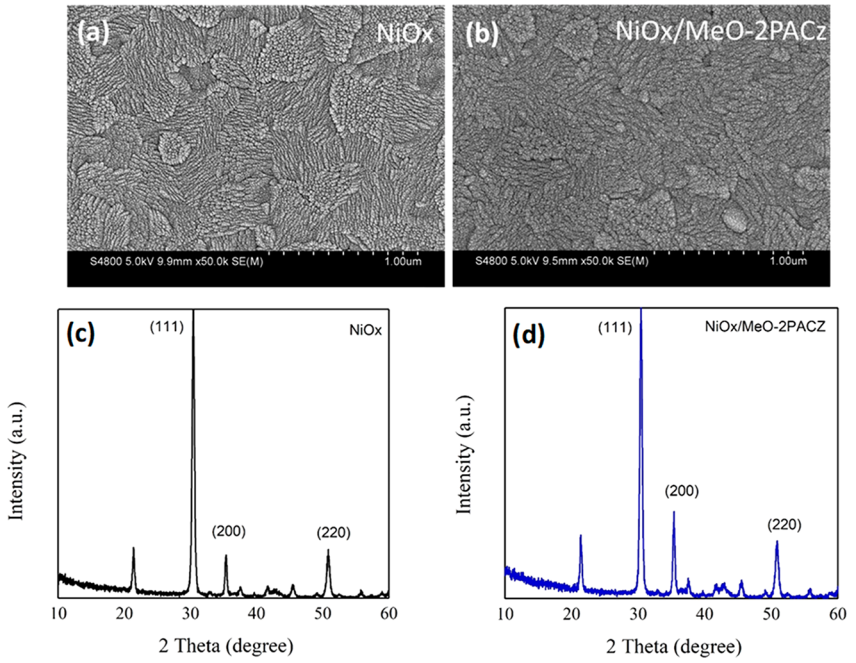

Figure 2. (a, b) SEM images of NiO_x before and after treatment with MeO-2PACz SAM, (c) XRD patterns for NiO_x and (d) XRD patterns for NiO_x/MeO-2PACz SAM.

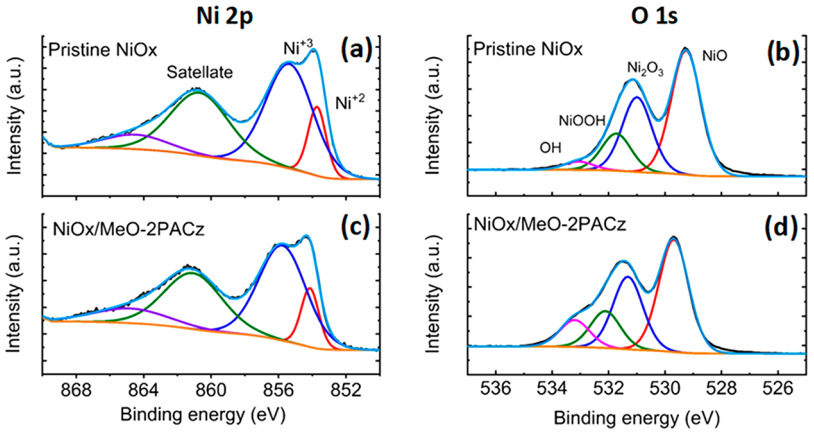

Figure 3. XPS surface spectra: (a) Ni 2p3/2 for pristine NiO_x, (b) O 1s for pristine NiOx, (c) Ni 2p3/2 for NiO_x treated with MeO-2PACz, and (d) O 1s for NiO_x treated with MeO-2PACz.

crystallization of the NiO_x film, as well as the interaction between NiO_x and MeO-2PACz.

3.1.1. Structural and Optical Characterization of NiO_x. Treatment of NiO_x with MeO-2PACz was investigated usingscanning electron microscopy (SEM), as shown in Figure 2a,b. The surface morphology of the pristine NiO_x film and treated NiO_x films were investigated, whereby minimal changes were observed. In this case, the results depict the same domain size and good coverage. Notably, the SEM images do not show a significant difference, implying that with or without the MeO-2PACz layer the morphological properties are retained.

The transmittance of NiO_x and NiO_x/MeO-2PACz was investigated, as shown in Figure S1, using UV−vis transmittance spectra. The same NiO_x substrate was measured before and after MeO-2PACz treatment to show the minimal change by the introduction of the SAM.

The crystallinity of the film was studied by XRD, and the results are presented in Figure 2c,d in which the evolution of the XRD patterns obtained for the NiO_x film and the field after being modified with MeO-2PACz are shown. The dominant (111), (200), and (220) peaks fit well to crystalline NiO.[59] Notably, in the two films, there are no significant changes, which means that the SAM of MeO-2PACz should not change the crystal structure of NiOx.

3.1.2. Surface Analysis for NiO_x. XPS was conducted to investigate the properties of NiO_x. In this case, the chemical components of the pristine NiO_x film and NiO_x/MeO-2PACz were analyzed. The characteristic peaks for Ni $2p_{3/2}$ and O 1s are presented in Figure 3. Furthermore, decomposition of the XPS spectrum shows that the Ni 2p spectrum can be fitted by two oxidation states, namely, Ni^{2+} and Ni^{3+}. The other two peaks are related to satellite peaks. Ni^{2+} is found at 853.7 and 854.1 eV for the pristine NiO_x and modified NiO_x surfaces, respectively, as shown in Figure 3a,c. This peak corresponds to NiO_6 octahedral bonding in the cubic rock salt NiO structure.[60] Another peak was observed at 855.3 eV for pristine NiO and at 855.7 eV for modified NiO_x, which can be attributed to Ni^{3+} comprising NiOOH[61] and Ni_2O_3.[59,62] In

https://doi.org/10.1021/acsomega.2c00509
ACS Omega 2022, 7, 12147−12157

previous studies, this peak has been assigned to the O vacancy in NiO_x.[15] The broad peaks observed at 860.6 and 864.4 eV are assigned to the shakeup processes (satellites) for NiO.[61,63] After treatment of the NiO film, a significant decrease occurs in the integrated area of overall Ni peaks, as summarized in Table 1. Notably, a shift of ~0.5 eV was observed for the dominant peaks in Ni $2p_{3/2}$ for pristine and treated NiO_x, implying that electron transfer occurs. This is similar to a previous result,[64] which shows a shift in the core component of NiO after treatment. In conclusion, the surface passivation cannot be supported by the XPS results. In addition, a high-resolution XP spectrum for the C 1s and N 1s is shown in the Figure S2. The position for C 1s peaks for pristine NiO_x is the first peak was obtained at 284.9 eV and can be assigned to the C−C bond, whereas the second peak was at 286.4 and can be identified as representing the C−O−C bond. A third peak is found at the position of 288.3 eV, which is related to C═O. Moreover, the NiO_x with MeO-2PACz layer has three C 1s peaks which are 284.9, 286.4, and 288.6 eV. Those peaks are related to C−C, C−O−C, and C═O, respectively. The N 1s spectrum was found in the NiOx with MeO-2PACz layer at 400.1 eV as shown in Figure S2.

Table 1. Summary of the Relative Intensity of the Ni 2p, O 1s, and P 2p Peaks Showing the Area under the Curve for the Pristine NiOx and NiO_x/MeO-2PACz Samples Obtained from XPS

		control (NiOx)		NiO_x/MeO-2PACz	
elements	peaks	position (eV)	integrated area (%)	position (eV)	integrated area (%)
Ni 2p	Ni^{2+} (NiO)	853.7	2.6	854.1	1.8
	Ni^{3+} (NiOOH), Ni_2O_3	855.3	10.8	855.7	7.8
O 1s	NiO (Ni^{2+})	529.2	21.8	529.6	18.2
	Ni_2O_3 (Ni^{3+})	530.9	13.1	531.3	11.7
	NiOOH	531.7	6.5	532.1	5.9
	OH	533.0	1.4	533.2	4.3
P 2p	$2P_{3/2}$			133.1	1.2
	$2P_{1/2}$			133.9	0.6

The binding energy in the O 1s spectra was resolved into four main oxygen states, as shown in Figure 3b,d. The peaks at 529.2 and 529.6 eV are attributed to NiO or Ni^{2+}[62] for pristine NiO_x and NiO_x/MeO-2PACz. Moreover, the peaks at 530.9 eV for pristine NiO_x and 531.3 eV for NiO_x/MeO-2PACz are assigned to O-bonded Ni_2O_3 or Ni^{3+}, as reported previously.[62] In addition, an increased amount of Ni_2O_3 has been reported to contribute to an increased work function (WF).[65] The peaks at 531.7 and 532.1 eV are related to NiOOH.[66−68] The higher binding energy at 533 eV is attributed to hydroxyl (OH) groups,[69] and the intensity of this peak increases after the treatment, which is probably because of the hydroxyl group present in the MeO-2PACz structure.

Evidence that the NiO_x surface was covered with MiO-2PACz after the treatment is indicated by the P 2p peak observed for the two phosphates and metaphosphate, as shown by the XPS spectra in Figure S2. Because the main P 2p binding energy is 133.1 eV, this peak is attributed to phosphate groups, which indicates a phosphorus binding state.[62]

3.2. Understanding the Role of MeO-2PACz (SAM) on a Perovskite Film. Understanding the impact of MeO-

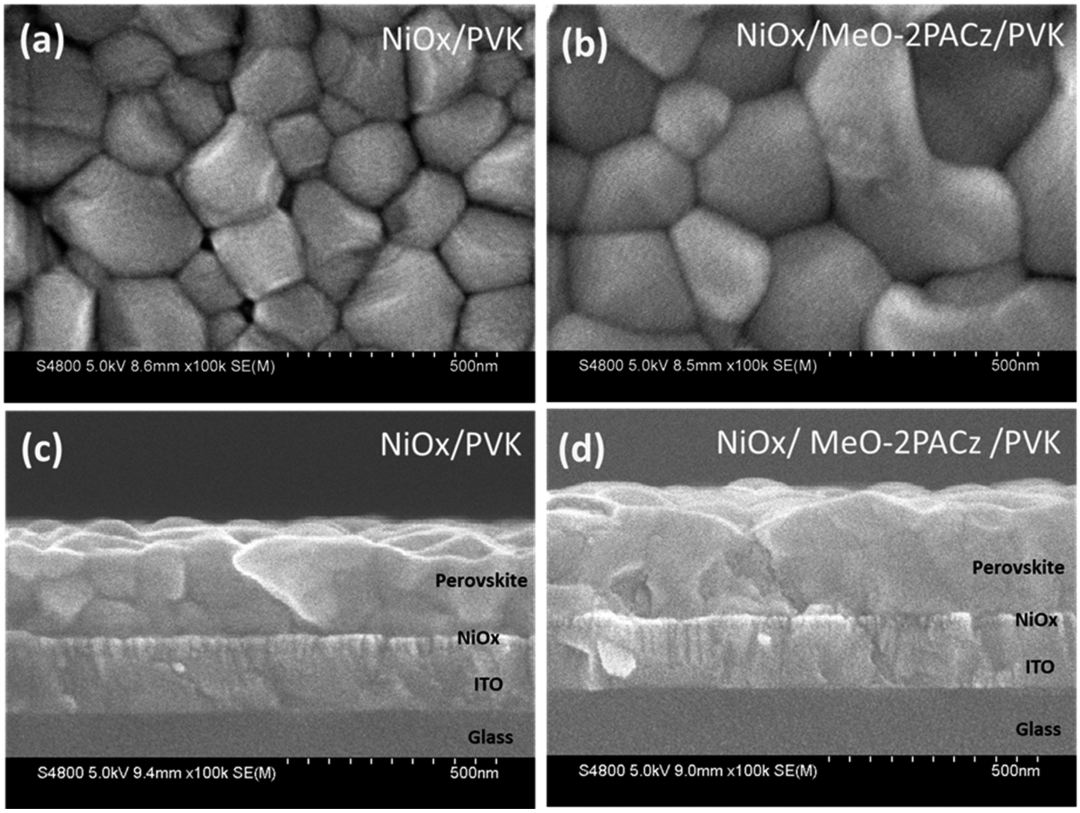

Figure 4. SEM images of perovskite (PVK) films: (a) top surface SEM without treatment, (b) top surface SEM with MeO-2PACz interface, (c) cross-sectional scanning image without treatment, (d) cross-sectional scanning image with a MeO-2PACz interface.

https://doi.org/10.1021/acsomega.2c00509
ACS Omega 2022, 7, 12147−12157

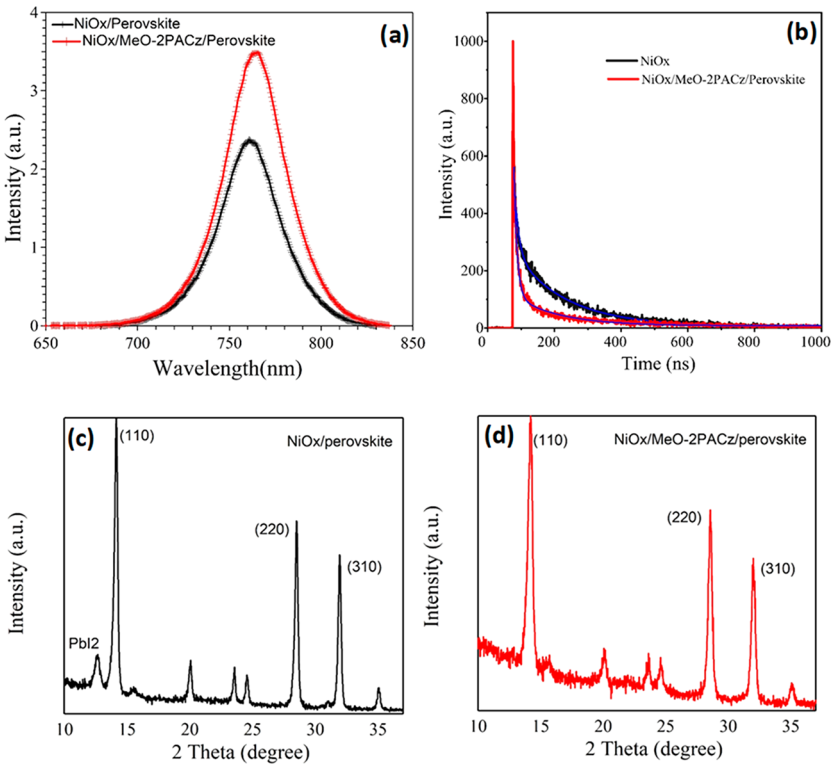

Figure 5. Steady-state PL for perovskite films with and without treatment (a), TRPL measured for perovskite films with and without treatment (b), and XRD patterns for perovskite films on pristine NiO_x (c) and XRD for modified NiO_x(d).

2PACz (SAM) on the performance of perovskite devices requires investigating the morphology and optical properties of perovskite films. Additionally, the defect level at the NiO_x/MeO-2PACz interface and the effect of the treatment on the energy level are investigated.

3.2.1. Effect of Surface Modification on the Morphology of Perovskite Film and the Optical Properties of Perovskite Film after Treatment of NiO_x. SEM analysis was carried out to gain insights into the perovskite morphology on NiO_x and NiO_x/MeO-2PACz, as shown in Figure 4a−d. A significant difference in perovskite domain size when deposited onto the MeO-2PACz layer is obtained from the quantified domain size. Based on the surface SEM images, an increase in domain size is observed because of the MeO-2PACz interface layer. Hence, treating NiO_x with MeO-2PACz influences the perovskite's bulk properties with uniform perovskite crystallinity because of the passivation of the surface defect in NiO_x, leading to a slight enhancement in domain size; here, suppression of recombination is expected. SEM images of the cross-section of samples with a layered structure ITO/NiO_x/MeO-2PACz/perovskite indicates no significant morphological difference for the perovskite.

Steady-state PL and TRPL were performed to investigate the photophysical properties of perovskite films with and without the MeO-2PACz interface layer. Figure 5a shows the PL results obtained for the perovskite films. The PL intensities are increased after MeO-2PACz treatment, which indicates a significant suppression of recombination in the perovskite layer.[70] Further measurements included TRPL analysis, which aimed to understand the recombination lifetime in perovskites. The results are illustrated in Figure 5b, which shows the control perovskite device and modified film with a MeO-2PACz layer. A single wavelength of 402 nm was applied as an excitation source. Figure 5b shows the faster decay reflecting the Förster charge injection into the MeO-2PACz-treated interface. Effective transfer of the charge carrier was attained for the modified sample according to the TRPL results. A higher steady-state PL indicates slightly better surface passivation; thus, the faster TRPL decay likely stems from charge transfer and not higher nonradiative recombination.

The PL and TRPL results indicate the role of the MeO-2PACz layer in surface passivation. Hence, these results explain the enhancement of the J_{sc} for MeO-2PACz-modified PSCs, which will be discussed later.

The XRD results for perovskite films with and without the MeO-2PACz layer are presented in Figure 5c,d, which indicates the effect of MeO-2PACz on the surface. In this case, the diffraction peaks for the perovskite layer with the MeO-2PACz treatment are similar to the control film without a MeO-2PACz layer. However, a new diffraction peak appears at 12°, which is attributed to PbI_2, which indicates the presence of unreacted PbI_2 content in the perovskite film. Introducing the MeO-2PACz interface layer between perovskite/NiO_x results in the total disappearance of PbI_2 crystals, which can be explained by their conversion in the perovskite phase.

The XRD results obtained lead to the conclusion that NiO_x without treatment affects the perovskite film because of the improper perovskite crystallization on NiO_x without a MeO-2PACz underlayer, hence resulting in the appearance of residual PbI_2 that appears unclear. However, the presence of H_2O and OH groups and interstitial oxygen on NiO_x or the presence of Ni^{3+} in NiO_x can cause improper perovskite crystallization.[15,18,71,72] On the other hand, the device containing the MeO-2PACz interface layer shows a better passivation effect than perovskite/NiO_x. Thus, the MeO-

https://doi.org/10.1021/acsomega.2c00509
ACS Omega 2022, 7, 12147−12157

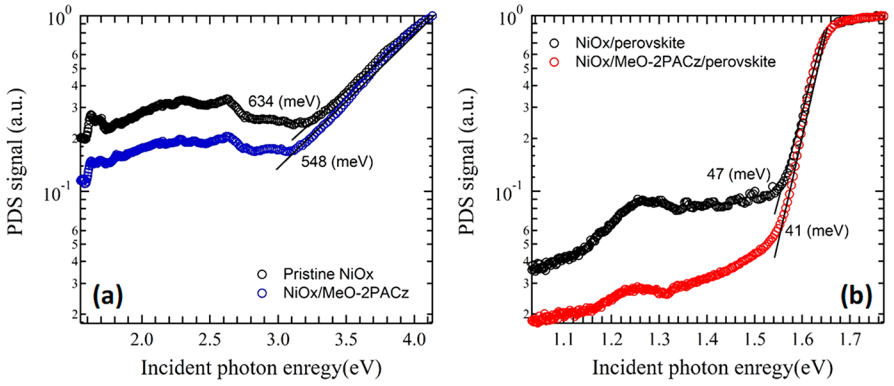

Figure 6. PDS spectra and the Urbach energy as determined from the inverse slope of the PDS signals for (a) NiOx and (b) perovskite.

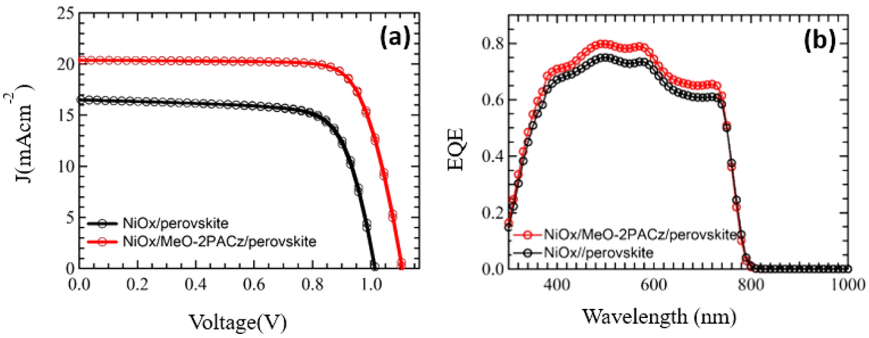

Figure 7. (a) Representative current density−voltage ($J-V$) characteristics for the control perovskite device and the device modified using the MeO-2PACz interface layer. (b) EQE spectra for the control perovskite device and the device modified with a MeO-2PACz interface layer. Integrated Jsc for the MeO-2PACz treated and untreated devices are 17.7 and 16.3 mA/cm^2, respectively.

Table 2. Device Parameters for Perovskite Solar Cells Including the Control Devices and Devices Modified Using a SAM Layer Interface[a]

device	Jsc (mA/cm^2)	Voc (V)	FF (%)	R_s (Ω·cm^2)	R_{sh} (Ω·cm^2)	η (%)
perovskite/NiO_x	17.3 ± 0.68	1.0 ± 0.06	0.7 ± 0.03	8.7 ± 2.08	1027.5 ± 334.78	11.9 ± 0.74
perovskite/MeO-2PACz/NiO_x	20.1 ± 0.18	1.11 ± 0.01	0.8 ± 0.01	4.8 ± 0.45	4810.7 ± 437.98	17.2 ± 0.03

[a]The results are derived from the eight perovskite solar cells for each condition.

2PACz layer was utilized to passivate the defects in the perovskite layer.

3.2.2. Studying the Defect Level at the Interface. To further support our claim that the MeO-2PACz layer can passivate the NiO_x surface, PDS was applied to further investigate the pristine NiO_x and NiO_x/perovskites; the results obtained are compared with MeO-2PACz-treated NiO_x, as shown in Figure 6a,b. The intensity of the PDS signal measured for NiO_x without treatment is higher than that of the treated samples. Moreover, the slope of the spectrum depicts the structural order of the surface. A quantitative description of disorder is indicated by the Urbach energy, which is described as the inverse slope of the PDS signal. PDS signals are observed to range from 4 to 3.2 eV, as shown in Figure 6a, and from 1.65 eV to ∼1.7 eV, as shown in Figure 6b, which indicate a reduction of the defect level at the NiOx surfaces and NiOx/perovskite interface, respectively. Conversely, the Urbach energy shows a decline in value with treated NiO_x, which indicates a reduction in the defect level.[73,74] We can conclude that the MeO-2PACz layer can passivate the surface of NiO_x, improving the crystalline quality and decreasing the number of defects.

3.3. Effect of Surface Modification on Photovoltaic Properties. The effects of surface modification were investigated, as shown in Figure 7a,b. Figure 7a represents the current $J-V$, a characteristic control for a perovskite device and a modified device with a MeO-2PACz SAM layer. Figure 7b shows the external quantum efficiency (EQE) spectra for the control perovskite device and modified device with the SAM layer.

The results are summarized in Table 2, indicating the average device parameters for PSCs, whereby the data for the control device and device modified with the MeO-2PACz interface layer are presented. The average results are derived from measurements for eight perovskite solar cell devices for each condition (Figure S6).

The effect of film quality on carrier recombination was studied by comparing the photovoltaic performance of the fabricated devices with and without the MeO-2PACz treatment. The current $J-V$ characteristics with and without MeO-2PACz treatment were analyzed, as shown in Figure 7a. Notably, the PCEs for the devices with and without MeO-2PACz treatment were determined to be 17.2% and 11.9%, respectively. The devices were fabricated under the same conditions, and the results are summarized in Table 2. The

https://doi.org/10.1021/acsomega.2c00509
ACS Omega 2022, 7, 12147−12157

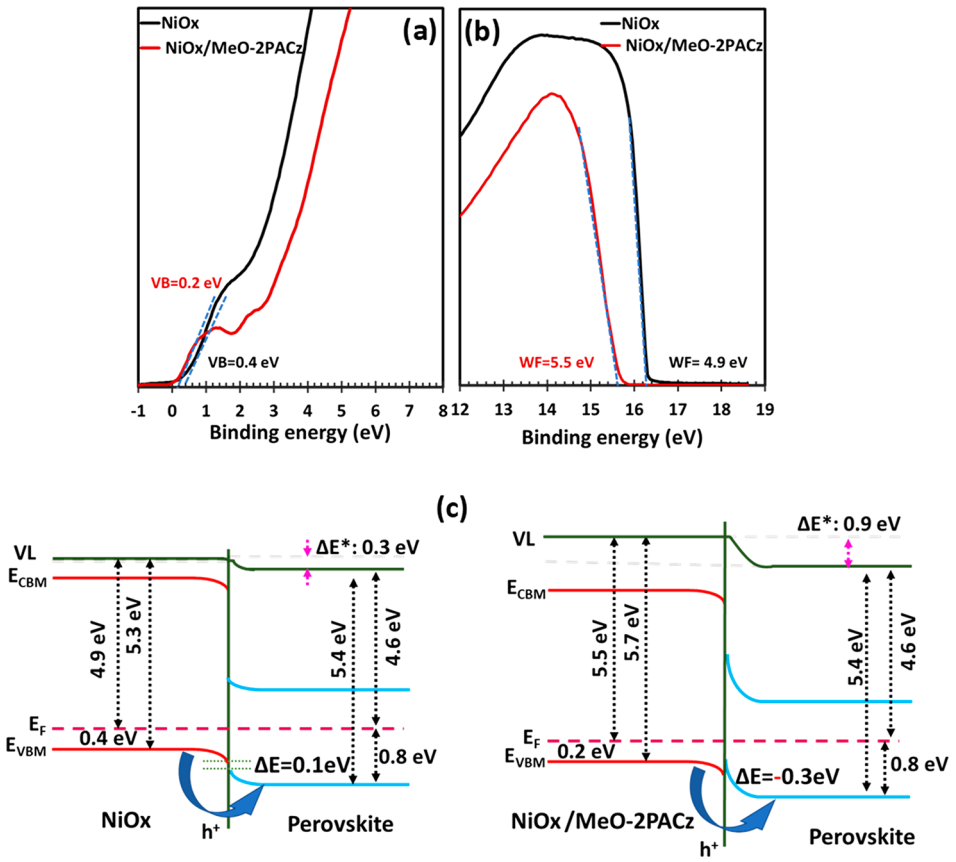

Figure 8. UPS spectra for NiO_x and NiO_x/MeO-2PACz, as measured under a bias of −10 V. (a) Valence band spectra for NiO_x and NiO_x/MeO-2PACz. (b) Work function (φ) is calculated using the equation $\varphi = h\nu$; the secondary electron (SE) is used as the cut off. (c) Energy level diagram for pristine NiOx (left) and NiO_x/MeO-2PACz (right).

results indicate that there is a significant enhancement of V_{oc}, J_{sc}, FF, and R_{sh} obtained for the MeO-2PACz-treated device when compared with the untreated device. The certified data for the MeO-2PACz-treated device are shown in Figure S3 with efficiency of 16.25%. The preliminary stability testing over 100 h was also conducted under maximum power point tracking (MPPT) conditions. The MeO-2PACz-treated and untreated devices revealed similar performance as shown in Figure S4, showing almost no reduction in the power conversion efficiencies.

The EQE was measured to study the efficiency of photocurrent conversion. The results show that the EQE covers the entire visible range from 300 to 800 nm for the treated devices and control device, as presented in Figure 7b. The results confirm that the MeO-2PACz-treated device has a higher EQE than the control device, and bandgap energies for both devices are about 1.55 eV that which is typical value for MAPI perovskites.

An analysis of the internal quantum energy (IQE) measurements for the devices was conducted, and the results are presented in Figure S5. The values obtained correspond to the ratio of the carrier charge, which is collected by the solar cell, to the number of photons absorbed under illumination. The results show that the charge carriers generated and collected for solar cell operation are significantly higher when the perovskite device is treated with MeO-2PACz.

3.4. Electronic Properties and Energy Level for Perovskite Films. To determine the mechanism behind this improvement, the electronic structures of NiO_x with and without a MeO-2PACz interlayer were investigated using ultraviolet photoelectron spectroscopy (UPS). The UPS results for NiO_x and NiO_x/MeO-2PACz, as measured under a −10 V bias for the valence band (VB), are shown in Figure 8a, and the secondary electrons are shown in Figure 8b. Additionally, the WF for pristine NiO_x and NiO_x covered with MeO-2PACz was determined to be 4.9 and 5.5 eV, respectively.

The obtained VB values for perovskite on NiO_x and NiO_x/MeO-2PACz are close to the Femi level, which improves the device performance by facilitating charge transfer between perovskites and NiO_x, as shown in Figure 8c. The values of the WF and IE for the perovskite layer were taken from literature.[25] Before MeO-2PACz treatment, an energy gap of 0.1 eV between the VBM of perovskite and the VBM of NiO_x can be observed, which can lead to the formation of a hole trap at the interface for charge carriers with insufficient kinetic energy to overcome the gap. After NiO_x was treated with MeO-2PACz, the VBM of perovskite exceeded the VBM of NiO_x. Thus, the energy gap is compensated due to an energy shift, resulting in a proper energy level alignment for hole transport over the interface. The energetic gap between the VBM of perovskite and NiO_x changes from +0.1 eV to −0.3 eV. More details for the extraction of these values can be found in Table S3.

4. CONCLUSIONS

In the current study, we modified a hole transport layer (NiO_x) with a MeO-2PACz (SAM) layer. Inserting the MeO-2PACz

https://doi.org/10.1021/acsomega.2c00509
ACS Omega 2022, 7, 12147−12157

interface between a NiO_x hole transport layer and perovskite layer helped decrease defects by passivation of NiO_x. On the basis of the results obtained, the MeO-2PACz on NiO_x interface significantly improves the defect level and device performance. This improvement in performance can be attributed to a reduction in charge recombination, increase in extraction efficiency, and enhancement of the perovskite film quality with its large domain size. The analysis further indicates that, generally, the introduction of MeO-2PACz results in the passivation of NiO_x surface defects, resulting in an enhancement of the crystallization. In summary, interface modification leads to various positive effects, including better interfacial contact, better energy level alignment, enhanced crystallization, and an increase in the power conversion efficiency. Thus, our results offer a promising mechanism for improving the performance of inorganic carrier transport layers in PSCs, which can potentially be extended to other combinations of inorganic semiconductors and functional organic molecule dopants in the future.

■ ASSOCIATED CONTENT

Supporting Information

The Supporting Information is available free of charge at https://pubs.acs.org/doi/10.1021/acsomega.2c00509.

Data analysis for the XPS spectra obtained from NiOx; electronic properties and energy level for perovskite films (PDF)

■ AUTHOR INFORMATION

Corresponding Authors

Masatoshi Yanagida − *Photovoltaic Materials Group, Center for GREEN Research on Energy and Environmental Materials, National Institute for Materials Science (NIMS), Tsukuba, Ibaraki 305-0044, Japan;* orcid.org/0000-0002-8065-7875; Email: yanagida.masatoshi@nims.go.jp

Yasuhiro Shirai − *Photovoltaic Materials Group, Center for GREEN Research on Energy and Environmental Materials, National Institute for Materials Science (NIMS), Tsukuba, Ibaraki 305-0044, Japan;* orcid.org/0000-0003-2164-5468; Email: shirai.yasuhiro@nims.go.jp

Authors

Amira R. M. Alghamdi − *Photovoltaic Materials Group, Center for GREEN Research on Energy and Environmental Materials, National Institute for Materials Science (NIMS), Tsukuba, Ibaraki 305-0044, Japan; Flinders Institute for Nanoscale Science and Technology, Flinders University, Adelaide, SA 5001, Australia; Department of Physics, College of Science, Imam Abdulrahman Bin Faisal University, 31441 City Dammam, Saudi Arabi*

Gunther G. Andersson − *Flinders Institute for Nanoscale Science and Technology, Flinders University, Adelaide, SA 5001, Australia;* orcid.org/0000-0001-5742-3037

Kenjiro Miyano − *Photovoltaic Materials Group, Center for GREEN Research on Energy and Environmental Materials, National Institute for Materials Science (NIMS), Tsukuba, Ibaraki 305-0044, Japan;* orcid.org/0000-0002-5869-3087

Complete contact information is available at: https://pubs.acs.org/10.1021/acsomega.2c00509

Notes

The authors declare no competing financial interest.

■ ACKNOWLEDGMENTS

A.R.M.A. and G.G.A. thank the National Institute for Material Science (NIMS), Japan, and Flinders University, Adelaide, for International Cooperative Graduate Program (ICGP) fellowships. The authors are grateful to Dr. Masatomo Sumiya for collecting the PDS data.

■ REFERENCES

(1) Eperon, G. E.; Burlakov, V. M.; Goriely, A.; Snaith, H. J. Neutral color semitransparent microstructured perovskite solar cells. *ACS Nano* **2014**, *8*, 591−598.

(2) Snaith, H. J. Perovskites: the emergence of a new era for low-cost, high-efficiency solar cells. *J. Phys. Chem. Lett.* **2013**, *4*, 3623−3630.

(3) Ye, S.; Rao, H.; Yan, W.; Li, Y.; Sun, W.; Peng, H.; Liu, Z.; Bian, Z.; Li, Y.; Huang, C. A strategy to simplify the preparation process of perovskite solar cells by co-deposition of a hole-conductor and a perovskite layer. *Adv. Mater.* **2016**, *28*, 9648−9654.

(4) Hu, L.; Wang, W.; Liu, H.; Peng, J.; Cao, H.; Shao, G.; Xia, Z.; Ma, W.; Tang, J. PbS colloidal quantum dots as an effective hole transporter for planar heterojunction perovskite solar cells. *J. Mater. Chem. A* **2015**, *3*, 515−518.

(5) Xiao, Z.; Dong, Q.; Bi, C.; Shao, Y.; Yuan, Y.; Huang, J. Solvent annealing of perovskite-induced crystal growth for photovoltaic-device efficiency enhancement. *Adv. Mater.* **2014**, *26*, 6503−6509.

(6) Wu, Z.; Bai, S.; Xiang, J.; Yuan, Z.; Yang, Y.; Cui, W.; Gao, X.; Liu, Z.; Jin, Y.; Sun, B. Efficient planar heterojunction perovskite solar cells employing graphene oxide as hole conductor. *Nanoscale* **2014**, *6*, 10505−10510.

(7) Wang, Q.; Bi, C.; Huang, J. Doped hole transport layer for efficiency enhancement in planar heterojunction organolead trihalide perovskite solar cells. *Nano Energy* **2015**, *15*, 275−280.

(8) Nakai, H.; Sugiyama, M.; Chichibu, S. F. Ultraviolet light-absorbing and emitting diodes consisting of a p-type transparent-semiconducting NiO film deposited on an n-type GaN homoepitaxial layer. *Appl. Phys. Lett.* **2017**, *110*, 181102.

(9) Aydin, E.; Troughton, J.; De Bastiani, M.; Ugur, E.; Sajjad, M.; Alzahrani, A.; Neophytou, M.; Schwingenschlögl, U.; Laquai, F.; Baran, D. Room-temperature-sputtered nanocrystalline nickel oxide as hole transport layer for p-i-n perovskite solar cells. *ACS Appl. Energy Mater.* **2018**, *1*, 6227−6233.

(10) Hu, Z.; Chen, D.; Yang, P.; Yang, L.; Qin, L.; Huang, Y.; Zhao, X. Sol-gel-processed yttrium-doped NiO as hole transport layer in inverted perovskite solar cells for enhanced performance. *Appl. Surf. Sci.* **2018**, *441*, 258−264.

(11) Wang, S.; Zhang, B.; Feng, D.; Lin, Z.; Zhang, J.; Hao, Y.; Fan, X.; Chang, J. Achieving high performance and stable inverted planar perovskite solar cells using lithium and cobalt co-doped nickel oxide as hole transport layers. *J. Mater. Chem. C* **2019**, *7*, 9270−9277.

(12) Liu, Z.; Chang, J.; Lin, Z.; Zhou, L.; Yang, Z.; Chen, D.; Zhang, C.; Liu, S.; Hao, Y. High-Performance Planar Perovskite Solar Cells Using Low Temperature, Solution-Combustion-Based Nickel Oxide Hole Transporting Layer with Efficiency Exceeding 20%. *Adv. Energy Mater.* **2018**, *8*, 1703432.

(13) Li, W.; Zhang, W.; Van Reenen, S.; Sutton, R. J.; Fan, J.; Haghighirad, A. A.; Johnston, M. B.; Wang, L.; Snaith, H. J. Enhanced UV-light stability of planar heterojunction perovskite solar cells with caesium bromide interface modification. *Energy Environ. Sci.* **2016**, *9*, 490−498.

(14) Zhou, L.; Lin, Z.; Ning, Z.; Li, T.; Guo, X.; Ma, J.; Su, J.; Zhang, C.; Zhang, J.; Liu, S. Highly efficient and stable planar perovskite solar cells with modulated diffusion passivation toward high power conversion efficiency and ultrahigh fill factor. *Solar RRL* **2019**, *3*, 1900293.

(15) Cui, J.; Meng, F.; Zhang, H.; Cao, K.; Yuan, H.; Cheng, Y.; Huang, F.; Wang, M. CH3NH3PbI3-based planar solar cells with magnetron-sputtered nickel oxide. *ACS Appl. Mater. Interface.* **2014**, *6*, 22862−22870.
(16) Kim, B. G.; Jang, W.; Wang, D. H. Facile niox sol-gel synthesis depending on chain length of various solvents without catalyst for efficient hole charge transfer in perovskite solar cells. *Polymers* **2018**, *10*, 1227.
(17) Yang, H.; Park, H.; Kim, B.; Park, C.; Jeong, S.; Chae, W.-S.; Kim, W.; Jeong, M.; Ahn, T. K.; Shin, H. Unusual Hole Transfer Dynamics of the NiO Layer in Methylammonium Lead Tri-iodide Absorber Solar Cells. *J. Phys. Chem. Lett.* **2021**, *12*, 2770−2779.
(18) Yanagida, M.; Shimomoto, L.; Shirai, Y.; Miyano, K. Effect of carrier transport in NiO on the photovoltaic properties of lead iodide perovskite solar cells. *Electrochem.* **2017**, *85*, 231−235.
(19) Islam, M. B.; Yanagida, M.; Shirai, Y.; Nabetani, Y.; Miyano, K. NiOx hole transport layer for perovskite solar cells with improved stability and reproducibility. *ACS Omega* **2017**, *2*, 2291−2299.
(20) Islam, M. B.; Yanagida, M.; Shirai, Y.; Nabetani, Y.; Miyano, K. Highly stable semi-transparent MAPbI3 perovskite solar cells with operational output for 4000 h. *Sol. Energy Mater. Sol. Cells* **2019**, *195*, 323−329.
(21) Dubey, P.; Kaurav, N.; Devan, R. S.; Okram, G.; Kuo, Y. The effect of stoichiometry on the structural, thermal and electronic properties of thermally decomposed nickel oxide. *RSC Adv.* **2018**, *8*, 5882−5890.
(22) Corani, A.; Li, M.-H.; Shen, P.-S.; Chen, P.; Guo, T.-F.; El Nahhas, A.; Zheng, K.; Yartsev, A.; Sundström, V.; Ponseca, C. S., Jr Ultrafast dynamics of hole injection and recombination in organometal halide perovskite using nickel oxide as p-type contact electrode. *J. Phys. Chem. Lett.* **2016**, *7*, 1096−1101.
(23) Chen, W.; Wu, Y.; Fan, J.; Djurišić, A. B.; Liu, F.; Tam, H. W.; Ng, A.; Surya, C.; Chan, W. K.; Wang, D. Perovskite Solar Cells: Understanding the Doping Effect on NiO: Toward High-Performance Inverted Perovskite Solar Cells. *Adv. Energy Mater.* **2018**, *8*, 1870091.
(24) Chen, W.; Liu, F. Z.; Feng, X. Y.; Djurišić, A. B.; Chan, W. K.; He, Z. B. Cesium doped NiOx as an efficient hole extraction layer for inverted planar perovskite solar cells. *Adv. Energy Mater.* **2017**, *7*, 1700722.
(25) Chen, W.; Zhou, Y.; Wang, L.; Wu, Y.; Tu, B.; Yu, B.; Liu, F.; Tam, H. W.; Wang, G.; Djurišić, A. B. Molecule-doped nickel oxide: verified charge transfer and planar inverted mixed cation perovskite solar cell. *Adv. Mater.* **2018**, *30*, 1800515.
(26) Lany, S.; Osorio-Guillén, J.; Zunger, A. Origins of the doping asymmetry in oxides: Hole doping in NiO versus electron doping in ZnO. *Phys. Rev. B* **2007**, *75*, 241203.
(27) Zhang, K. H.; Xi, K.; Blamire, M. G.; Egdell, R. G. P-type transparent conducting oxides. *J. Phys.: Cond. Matt.* **2016**, *28*, 383002.
(28) Chen, W.; Wu, Y.; Yue, Y.; Liu, J.; Zhang, W.; Yang, X.; Chen, H.; Bi, E.; Ashraful, I.; Grätzel, M. Efficient and stable large-area perovskite solar cells with inorganic charge extraction layers. *Science* **2015**, *350*, 944−948.
(29) Kim, J. H.; Liang, P. W.; Williams, S. T.; Cho, N.; Chueh, C. C.; Glaz, M. S.; Ginger, D. S.; Jen, A. K. Y. High-performance and environmentally stable planar heterojunction perovskite solar cells based on a solution-processed copper-doped nickel oxide hole transporting layer. *Adv. Mater.* **2015**, *27*, 695−701.
(30) Li, G.; Jiang, Y.; Deng, S.; Tam, A.; Xu, P.; Wong, M.; Kwok, H. S. Overcoming the limitations of sputtered nickel oxide for high-efficiency and large-area perovskite solar cells. *Adv. Sci.* **2017**, *4*, 1700463.
(31) Shi, J.; Xu, X.; Li, D.; Meng, Q. Interfaces in perovskite solar cells. *Small* **2015**, *11*, 2472−2486.
(32) Wang, Q.; Chueh, C. C.; Zhao, T.; Cheng, J.; Eslamian, M.; Choy, W. C.; Jen, A. K. Effects of Self Assembled Monolayer Modification of Nickel Oxide Nanoparticles Layer on the Performance and Application of Inverted Perovskite Solar Cells. *CnemSusChem.* **2017**, *10*, 3794−3803.
(33) Yang, X.; Ying, Z.; Yang, Z.; Xu, J. R.; Wang, W.; Wang, J.; Wang, Z.; Yao, L.; Yan, B.; Ye, J. Light-Promoted Electrostatic Adsorption of High-Density Lewis Base Monolayers as Passivating Electron-Selective Contacts. *Adv. Sci.* **2021**, *8*, 2003245.
(34) Love, J. C.; Estroff, L. A.; Kriebel, J. K.; Nuzzo, R. G.; Whitesides, G. M. Self-assembled monolayers of thiolates on metals as a form of nanotechnology. *Chem. Rev.* **2005**, *105*, 1103−1170.
(35) Ulman, A. Formation and structure of self-assembled monolayers. *Chem. Rev.* **1996**, *96*, 1533−1554.
(36) Ali, F.; Roldán-Carmona, C.; Sohail, M.; Nazeeruddin, M. K. Applications of Self-Assembled Monolayers for Perovskite Solar Cells Interface Engineering to Address Efficiency and Stability. *Adv. Energy Mater.* **2020**, *10*, 2002989.
(37) Magomedov, A.; Al-Ashouri, A.; Kasparavičius, E.; Strazdaite, S.; Niaura, G.; Jošt, M.; Malinauskas, T.; Albrecht, S.; Getautis, V. Self-assembled hole transporting monolayer for highly efficient perovskite solar cells. *Adv. Energy Mater.* **2018**, *8*, 1801892.
(38) Caliò, L.; Follana-Berná, J.; Kazim, S.; Madsen, M.; Rubahn, H.-G.; Sastre-Santos, Á.; Ahmad, S. Cu (ii) and Zn (ii) based phthalocyanines as hole selective layers for perovskite solar cells. *Sustain. Energy Fuels* **2017**, *1*, 2071−2077.
(39) Más-Montoya, M.; Gómez, P.; Curiel, D.; da Silva, I.; Wang, J.; Janssen, R. A. A Self-Assembled Small-Molecule-Based Hole-Transporting Material for Inverted Perovskite Solar Cells. *Chem.—Eur. J.* **2020**, *26*, 10276−10282.
(40) Phung, N.; Verheijen, M.; Todinova, A.; Datta, K.; Verhage, M.; Al-Ashouri, A.; Köbler, H.; Li, X.; Abate, A.; Albrecht, S. Enhanced Self-Assembled Monolayer Surface Coverage by ALD NiO in p-i-n Perovskite Solar Cells. *ACS Appl. Mater. Interfaces* **2022**, *14*, 2166−2176.
(41) Bai, Y.; Chen, H.; Xiao, S.; Xue, Q.; Zhang, T.; Zhu, Z.; Li, Q.; Hu, C.; Yang, Y.; Hu, Z. Effects of a molecular monolayer modification of NiO nanocrystal layer surfaces on perovskite crystallization and interface contact toward faster hole extraction and higher photovoltaic performance. *Adv. Funct. Mater.* **2016**, *26*, 2950−2958.
(42) Zhang, J.; Luo, H.; Xie, W.; Lin, X.; Hou, X.; Zhou, J.; Huang, S.; Ou-Yang, W.; Sun, Z.; Chen, X. Efficient and ultraviolet durable planar perovskite solar cells via a ferrocenecarboxylic acid modified nickel oxide hole transport layer. *Nanoscale* **2018**, *10*, 5617−5625.
(43) Du, Y.; Xin, C.; Huang, W.; Shi, B.; Ding, Y.; Wei, C.; Zhao, Y.; Li, Y.; Zhang, X. Polymeric surface modification of NiO x-based inverted planar perovskite solar cells with enhanced performance. *ACS Sustain. Chem. Eng.* **2018**, *6*, 16806−16812.
(44) Di Girolamo, D.; Di Giacomo, F.; Matteocci, F.; Marrani, A. G.; Dini, D.; Abate, A. Progress, highlights and perspectives on NiO in perovskite photovoltaics. *Chem. Sci.* **2020**, *11*, 7746−7759.
(45) Głowienka, D.; Zhang, D.; Di Giacomo, F.; Najafi, M.; Veenstra, S.; Szmytkowski, J.; Galagan, Y. Role of surface recombination in perovskite solar cells at the interface of HTL/CH3NH3PbI3. *Nano Energy* **2020**, *67*, 104186.
(46) Boyd, C. C.; Shallcross, R. C.; Moot, T.; Kerner, R.; Bertoluzzi, L.; Onno, A.; Kavadiya, S.; Chosy, C.; Wolf, E. J.; Werner, J. Overcoming redox reactions at perovskite-nickel oxide interfaces to boost voltages in perovskite solar cells. *Joule* **2020**, *4*, 1759−1775.
(47) Mann, D. S.; Patil, P.; Kwon, S.-N.; Na, S.-I. Enhanced performance of pin perovskite solar cell via defect passivation of nickel oxide/perovskite interface with self-assembled monolayer. *Appl. Surf. Sci.* **2021**, *560*, 149973.
(48) Al-Ashouri, A.; Magomedov, A.; Roß, M.; Jošt, M.; Talaikis, M.; Chistiakova, G.; Bertram, T.; Márquez, J. A.; Köhnen, E.; Kasparavičius, E. Conformal monolayer contacts with lossless interfaces for perovskite single junction and monolithic tandem solar cells. *Energy Environ. Sci.* **2019**, *12*, 3356−3369.
(49) Al-Ashouri, A.; Köhnen, E.; Li, B.; Magomedov, A.; Hempel, H.; Caprioglio, P.; Márquez, J. A.; Vilches, A. B. M.; Kasparavicius, E.; Smith, J. A. Monolithic perovskite/silicon tandem solar cell with> 29% efficiency by enhanced hole extraction. *Science* **2020**, *370*, 1300−1309.

https://doi.org/10.1021/acsomega.2c00509
ACS Omega 2022, 7, 12147−12157

(50) Sun, J.; Shou, C.; Sun, J.; Wang, X.; Yang, Z.; Chen, Y.; Wu, J.; Yang, W.; Long, H.; Ying, Z. NiOx-Seeded Self-Assembled Monolayers as Highly Hole-Selective Passivating Contacts for Efficient Inverted Perovskite Solar Cells. *Solar RRL* **2021**, *5*, 2100663.
(51) Hotchkiss, P. J.; Jones, S. C.; Paniagua, S. A.; Sharma, A.; Kippelen, B.; Armstrong, N. R.; Marder, S. R. The modification of indium tin oxide with phosphonic acids: mechanism of binding, tuning of surface properties, and potential for use in organic electronic applications. *Acc. Chem. Res.* **2012**, *45*, 337−346.
(52) Zhang, H.; Cheng, J.; Lin, F.; He, H.; Mao, J.; Wong, K. S.; Jen, A. K.-Y.; Choy, W. C. Pinhole-free and surface-nanostructured NiO x film by room-temperature solution process for high-performance flexible perovskite solar cells with good stability and reproducibility. *ACS Nano* **2016**, *10*, 1503−1511.
(53) Boehm, H. Acidic and basic properties of hydroxylated metal oxide surfaces. *Disc. Faraday Soc.* **1971**, *52*, 264−275.
(54) Tripathi, N.; Yanagida, M.; Shirai, Y.; Miyano, K. Improved performance of planar perovskite devices via inclusion of ammonium acid iodide (AAI) derivatives using a two step inter-diffusion process. *J. Mater. Chem. C* **2019**, *7*, 3447−3451.
(55) Khadka, D. B.; Shirai, Y.; Yanagida, M.; Masuda, T.; Miyano, K. Enhancement in efficiency and optoelectronic quality of perovskite thin films annealed in MACl vapor. *Sustain. Energy Fuels* **2017**, *1*, 755−766.
(56) Upama, M. B.; Wright, M.; Puthen-Veettil, B.; Elumalai, N. K.; Mahmud, M. A.; Wang, D.; Chan, K. H.; Xu, C.; Haque, F.; Uddin, A. Analysis of burn-in photo degradation in low bandgap polymer PTB7 using photothermal deflection spectroscopy. *RSC Adv.* **2016**, *6*, 103899−103904.
(57) Sumiya, M.; Ueda, S.; Fukuda, K.; Asai, Y.; Cho, Y.; Sang, L.; Uedono, A.; Sekiguchi, T.; Onuma, T.; Honda, T. Valence band edge tail states and band gap defect levels of GaN bulk and In x Ga1- x N films detected by hard X-ray photoemission and photothermal deflection spectroscopy. *Appl. Phys. Exp.* **2018**, *11*, 021002.
(58) Sumiya, M.; Fukuda, K.; Yasiro, S.; Honda, T. Influence of thin MOCVD-grown GaN layer on underlying AlN template. *J. Cryst. Growth* **2020**, *532*, 125376.
(59) Islam, M. B.; Pant, N.; Yanagida, M.; Shirai, Y.; Miyano, K. Effect of hydroxyl groups in NiO x on the open circuit voltage of lead iodide perovskite solar cells. *Jpn. J. Appl. Phys.* **2018**, *57*, 08RE06.
(60) Chen, W.; Wu, Y.; Fan, J.; Djurišić, A. B.; Liu, F.; Tam, H. W.; Ng, A.; Surya, C.; Chan, W. K.; Wang, D. Understanding the doping effect on NiO: toward high-performance inverted perovskite solar cells. *Adv. Energy Mater.* **2018**, *8*, 1703519.
(61) Koushik, D.; Jošt, M.; Dučinskas, A.; Burgess, C.; Zardetto, V.; Weijtens, C.; Verheijen, M. A.; Kessels, W. M.; Albrecht, S.; Creatore, M. Plasma-assisted atomic layer deposition of nickel oxide as hole transport layer for hybrid perovskite solar cells. *J. Mater. Chem. C* **2019**, *7*, 12532−12543.
(62) Ivan, Ş.-B.; Popescu, I.; Fechete, I.; Garin, F.; Pârvulescu, V. I.; Marcu, I.-C. The effect of phosphorus on the catalytic performance of nickel oxide in ethane oxidative dehydrogenation. *Catal. Sci. Technol.* **2016**, *6*, 6953−6964.
(63) Sun, Y.; Chen, W.; Wu, Y.; He, Z.; Zhang, S.; Chen, S. A low-temperature-annealed and UV-ozone-enhanced combustion derived nickel oxide hole injection layer for flexible quantum dot light-emitting diodes. *Nanoscale* **2019**, *11*, 1021−1028.
(64) Tarasov, A.; Zhang, S.; Tsai, M. Y.; Campbell, P. M.; Graham, S.; Barlow, S.; Marder, S. R.; Vogel, E. M. Controlled doping of large-area trilayer MoS2 with molecular reductants and oxidants. *Adv. Mater.* **2015**, *27*, 1175−1181.
(65) Liu, S.; Liu, R.; Chen, Y.; Ho, S.; Kim, J. H.; So, F. Nickel oxide hole injection/transport layers for efficient solution-processed organic light-emitting diodes. *Chem. Mater.* **2014**, *26*, 4528−4534.
(66) Zhang, B.; Su, J.; Guo, X.; Zhou, L.; Lin, Z.; Feng, L.; Zhang, J.; Chang, J.; Hao, Y. NiO/Perovskite heterojunction contact engineering for highly efficient and stable perovskite solar cells. *Adv. Sci.* **2020**, *7*, 1903044.
(67) Pant, N.; Yanagida, M.; Shirai, Y.; Miyano, K. Effect of different surface treatments of sputtered NiO X on the photovoltaic parameters of perovskite solar cells: a correlation study. *Appl. Phys. Exp.* **2020**, *13*, 025505.
(68) Jiang, S.; Wu, Y.; Fang, D.-f.; Chen, Y. Hypothermic preconditioning but not ketamine reduces oxygen and glucose deprivation induced neuronal injury correlated with downregulation of COX-2 expression in mouse hippocampal slices. *J. Pharmacol. Sci.* **2018**, *137*, 30−37.
(69) Kwan, Y. C. G.; Ng, G. M.; Huan, C. H. A. Identification of functional groups and determination of carboxyl formation temperature in graphene oxide using the XPS O 1s spectrum. *Thin Solid Films* **2015**, *590*, 40−48.
(70) Chen, H.; Ye, F.; Tang, W.; He, J.; Yin, M.; Wang, Y.; Xie, F.; Bi, E.; Yang, X.; Grätzel, M. A solvent-and vacuum-free route to large-area perovskite films for efficient solar modules. *Nature* **2017**, *550*, 92−95.
(71) Lee, H.; Huang, Y.-T.; Horn, M. W.; Feng, S.-P. Engineered optical and electrical performance of rf-sputtered undoped nickel oxide thin films for inverted perovskite solar cells. *Sci, Rep.* **2018**, *8*, 1−10.
(72) Pant, N.; Kulkarni, A.; Yanagida, M.; Shirai, Y.; Miyasaka, T.; Miyano, K. Investigating the Growth of CH3NH3PbI3 Thin Films on RF-Sputtered NiOx for Inverted Planar Perovskite Solar Cells: Effect of CH3NH3+ Halide Additives versus CH3NH3+ Halide Vapor Annealing. *Adv. Mater. Interfaces* **2020**, *7*, 1901748.
(73) Wu, S.; Li, Z.; Zhang, J.; Liu, T.; Zhu, Z.; Jen, A. K.-Y. Efficient large guanidinium mixed perovskite solar cells with enhanced photovoltage and low energy losses. *Chem. Commun.* **2019**, *55*, 4315−4318.
(74) Li, Z.; Wu, S.; Zhang, J.; Yuan, Y.; Wang, Z.; Zhu, Z. Improving Photovoltaic Performance Using Perovskite/Surface-Modified Graphitic Carbon Nitride Heterojunction. *Solar RRL* **2020**, *4*, 1900413.

https://doi.org/10.1021/acsomega.2c00509
ACS Omega 2022, 7, 12147−12157